



New phosphor discovery by the single particle diagnosis approach

Takashi Takeda*, Naoto Hirosaki, Shiro Funahashi, Rong-Jun Xie

Sialon Unit, National Institute for Materials Science, Namiki 1-1, Tsukuba, Ibaraki 305-0044, Japan



ARTICLE INFO

Article history:

Received 21 August 2015

Received in revised form

10 November 2015

Accepted 13 November 2015

Available online 4 February 2016

Keywords:

Phosphor

Nitride

Oxynitride

Tiny single crystal

LEDs

ABSTRACT

New phosphors are required for the advancement of lighting and display technologies. One of the most effective ways for new phosphors is to employ new materials for host materials. It takes much time and labor to develop new materials from powder synthesis or single crystal growth. However, even if the powder product is a mixture phase, each particle is a single phase and a single crystal. The single particle diagnosis approach focuses on the tiny single crystal particle. Here we show the concept of the single particle diagnosis approach and some examples of new phosphor discovery by this approach.

© 2016 Elsevier Ltd. All rights reserved.

1. Introduction

New materials are always needed and in the field of phosphor research new phosphors are required for white light emitting diodes (white LEDs) application. White LEDs are now rapidly spreading to many applications (lighting, display backlight, car headlamp, etc.). It is composed of blue LED and phosphor. The mixture of luminescence from phosphor excited by LED and emission from the LED produce white light. The phosphor is a key material for governing the color characteristics of white LEDs (color rendering in the lighting, color reproduction in the backlight). Although the conventional white LED phosphor YAG:Ce has a high luminescence intensity, the luminescence spectrum is not suitable for high color rendering white LEDs in the lighting and the matching to the color filter is not good in the backlight. Alternative phosphors have been searched, and some Eu²⁺-doped Si, Al containing nitride and oxynitride (nitridosilicate, oxynitridosilicate, nitridoaluminosilicate, oxynitridoaluminosilicate) phosphors were found to have excellent luminescence properties for better color rendering and matching, and they have been commercialized [1–4]. New phosphors are still required for (1) the wide variation of emission spectra (peak position, peak width) to produce various types of white LEDs, (2) the coming change of emission wavelength of LEDs (near-UV LED) and (3) the high power LEDs where the thermal quenching of luminescence is more predominant.

In the synthesis of phosphors, a luminescent center is doped to a host material in small amount to obtain a luminescence. The luminescence property of Eu²⁺ or Ce³⁺ doped phosphor is so affected by the coordination environment of luminescent center. That is to say, the usage of different host material leads to new phosphor. The search for new phosphor is roughly classified to two methods. One is to employ a known crystal structure that is suitable for luminescent center doping and is not studied for host crystal [1–4]. The other is to find new host material by analyzing single crystals [5–14] or powder products [15]. Both methods, however, are definitely slow and labor intensive. In the single crystal analysis, a large size crystal with high purity and high quality (typically larger than 50–100 μm in all dimensions) is necessary to determine the crystal structure. It requires much time to grow the crystal especially for the material with high melting temperature or with no liquid phase. In the powder process, at least it is necessary to synthesize the new material as single phase to solve the crystal structure from powder XRD data. Even if the powder is single phase of new material, the complicated crystal structure is difficult to solve (i.e. crystal structure with large lattice parameter and low symmetry, crystal structure containing disorder). Therefore, it is desirable to find a way that allows the high-speed discovery of new phosphors, removing the need to prepare a perfect single crystal or a phase-pure powder. The combinatorial chemistry approach has been successfully utilized to high-throughput screening and optimizing luminescent materials [16–19]. However, the luminescent materials discovered so far cannot be considered as real “novel” phosphors as the crystal structure of end members are already known. The improved combinatorial synthesis method (heuristic

* Corresponding author.

E-mail address: TAKEDA.Takashi@nims.go.jp (T. Takeda).

optimization) greatly speeds up the discovery of new phosphors [20–22], but it still requires much times of synthesis for pure phase.

We have recently reported a highly effective method to discover new phosphor without special process for crystal growth and single phase powder, and named the new method “single particle diagnosis approach” [23,24]. Here we show the concept of the approach and some new phosphors discovered by this method.

2. Materials and methods

2.1. Concept and procedure of the approach

A single phase powder is obtained by synthesizing a single-phase composition in a phase diagram in a suitable synthesis condition. If the synthesized composition is a region of mixture phase, the product contains the particles of each phase. Actually, due to the non-homogeneity and non-equilibrium condition in a reaction vessel, the tendency to mixture phase will be increased. In the stage of new material research, most of the product is obtained as a mixture phase. However, even if the powder product is a mixture phase, focusing on each (isolated) particle, it is a single phase and a single crystal. In the single particle diagnosis approach, such particle is treated as a candidate of new phosphor. The schematic of single particle diagnosis approach is shown in Fig. 1.

Fig. 1(a) shows the powder samples of various compositions synthesized under standard process and they appear various types of emission by UV-LED excitation depending on the starting compositions. A microscope image of the powder in one crucible is shown in Fig. 1(b). Although the product seems to have a uniform orange luminescence, it consists of different types of luminescence

(yellow, orange, green, cyan, etc.), size and form in a micro-scale observation. Single crystal particles are picked and mounted on the glass capillary for the screening by single crystal XRD measurement (Fig. 1(c)). The lattice parameters and Bravais lattice are determined and compared to the database (ICSD, ICDD-PDF, etc.), and the candidates of new phosphor particle are selected. Emission spectrum by UV-LED excitation is supplementary used to judge the novelty of the particle. The glass particle and single crystal-like aggregate are ruled out in this stage.

The crystal structure of the new phosphor is then explored in detail with the EDS analysis (Fig. 1(d)). Due to the recent development of commercially available single crystal X-ray diffractometer (CCD or CMOS detector, focusing mirror), we can determine the crystal structure of a tiny microcrystal down to 5–10 μm. This microcrystal corresponds to the size synthesized by standard synthesis conditions. The special experiment for crystal growth is not necessary. Although much smaller crystal is analyzed by synchrotron XRD, there are many candidates in the single particle diagnosis approach and it is important to characterize them by the laboratory equipment.

Luminescent properties are also measured by single particle (Fig. 1(e)). Because the signal intensity from single particle is so weak, a microscopic observation is employed. We build a single particle fluorescence spectroscopy system to perform photoluminescence property measurements (emission and excitation spectra, thermal quenching, quantum efficiency (QE), decay) of a luminescent particle (Fig. 2). The accuracy of the system is acceptable for a fine particle, which is confirmed by using Ca- α -sialon:Eu²⁺ phosphor as a reference. Here the emission and QE results are shown. Due to the absence of reabsorption by other particles, the single

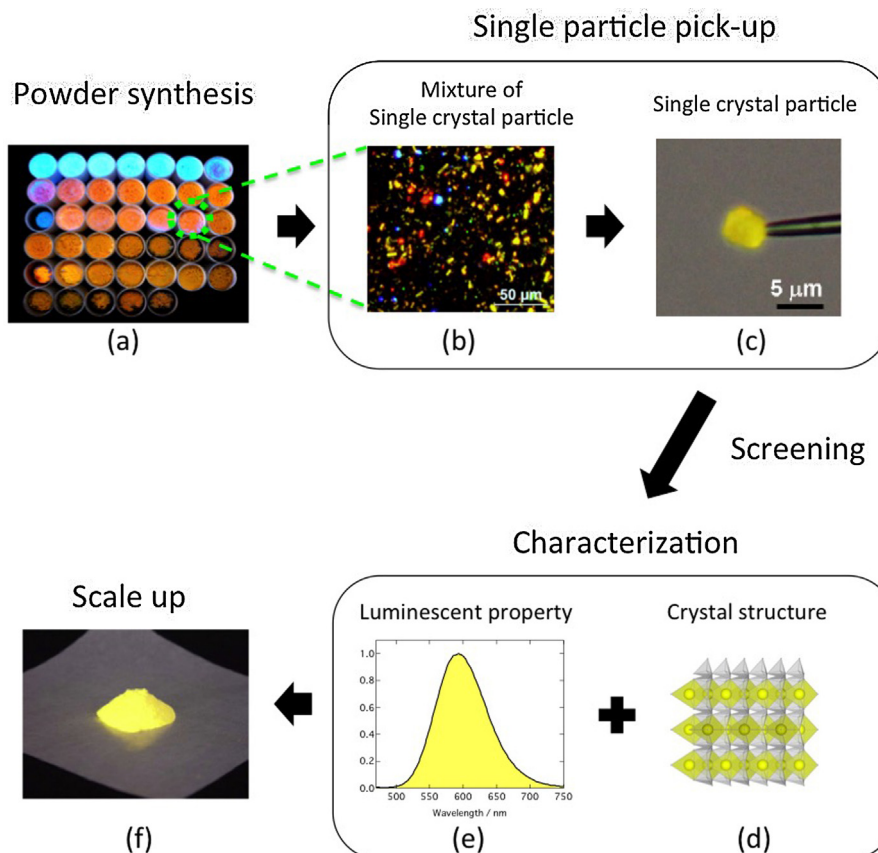


Fig. 1. Schematic of single particle diagnosis approach.

Adapted with permission from Ref. [23]. Copyright 2014 American Chemical Society.

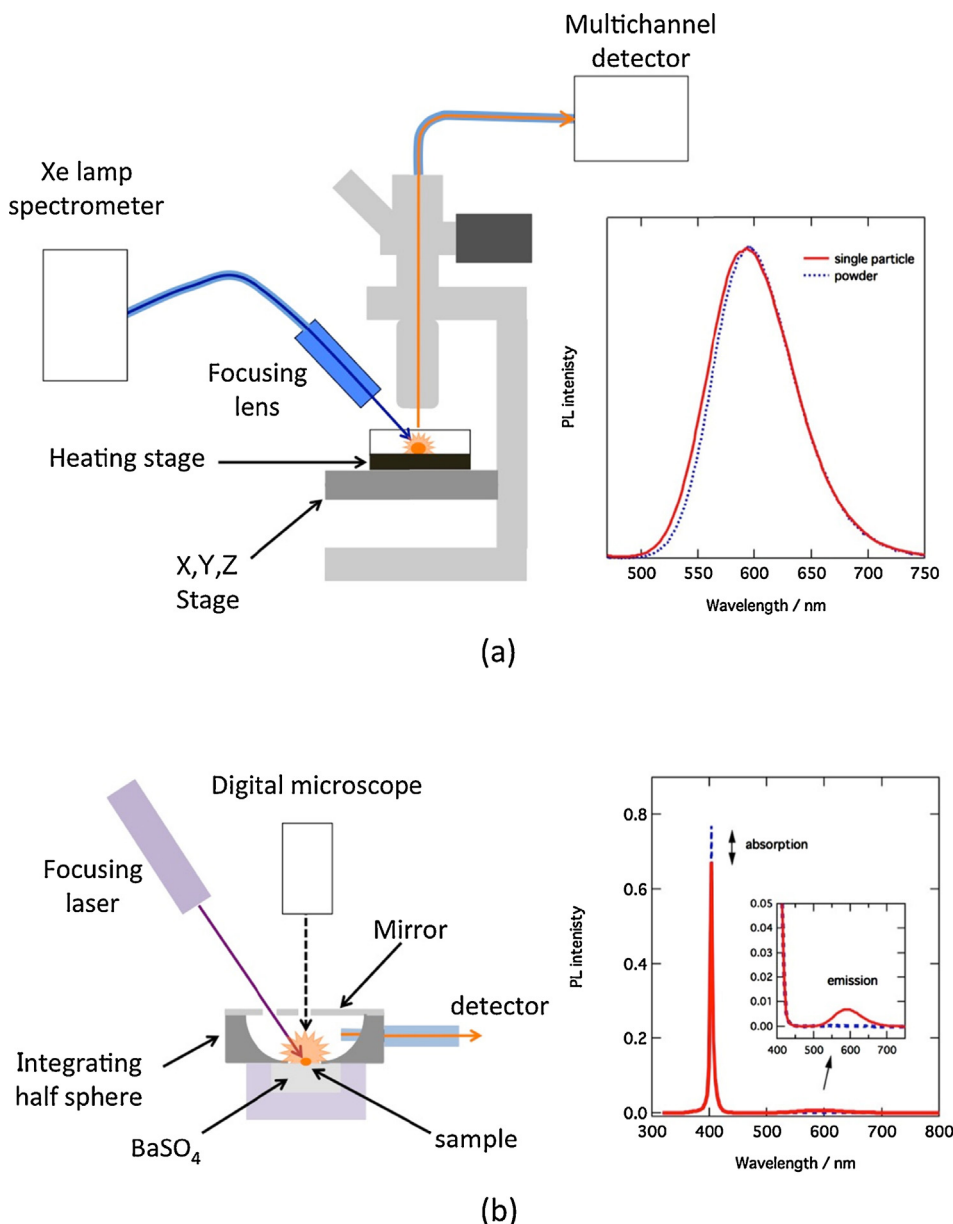


Fig. 2. Schematics of home-built single particle fluorescence microspectroscopy setups and measured spectra, (a) photoluminescence spectra and (b) quantum efficiency. Adapted with permission from Ref. [23]. Copyright 2014 American Chemical Society.

particle exhibited an emission band slightly blue-shifted at the left wing compared with the powder sample. In the QE measurement of the powder sample, the monochromatized Xe light is irradiated to the sample in an integrating sphere. QE is obtained by dividing the number of emission photons by the number of absorption photons. In a small crystal, the change of excitation light by particle's absorption is so small that it is difficult to obtain the accurate QE value. We use a focused laser (comparable to the particle size) and the reliable QE is obtained from a single crystal particle. Eventually, the new phosphor is synthesized as powder by reference to the information of analyzed composition (Fig. 1(f)).

The merit of this method is summarized as follows. (1) It is not necessary to synthesize the new phosphor as single phase powder. (2) It is not necessary to grow the new phosphor to large crystal. (3) The true luminescence property of the given composition is obtained because the one single crystal has no compositional and structural distribution as found in the powder sample. (4) A

small amount of new phosphor (including unintended new phosphor) in a powder sample is not overlooked because all produced particles are candidates. As the luminescence property is highly dependent on the crystal structure and composition, it is not difficult to select a particle from many candidate particles by using the luminescence as a clue. (5) The crystal orientation dependence is available (i.e. focused ion beam (FIB) processing for transmission electron microscope (TEM) observation of the desired lattice plane, crystal orientation dependence of luminescence).

2.2. Experimental

The mixed starting materials filled in a boron nitride crucible were fired in a nitrogen atmosphere of 1.0 MPa (Fujidempa Kogyo, FVPHR-R-10, FRET-40). XRD data of the selected and mounted single particle were collected using a diffractometer (Bruker-AXS, SMART APEX II Ultra) with Mo K α radiation ($\lambda = 0.71073 \text{ \AA}$) and

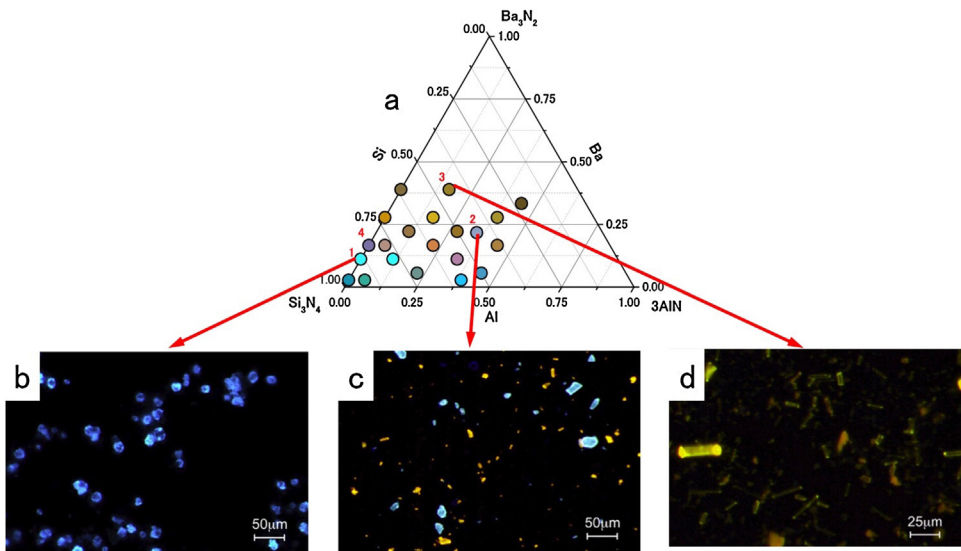


Fig. 3. (a) Phase diagram of the quasi-ternary Ba_3N_2 - Si_3N_4 - AlN system showing the compositions investigated and their intuitive emission colors. (b) Microscopic image of diamond-like blue-emitting phosphor particles (composition no. 1, $\text{Ba}:\text{Si}:\text{Al} = 0.11:0.89:0$) in a single phase powder. (c) Microscopic image of mixed luminescent particles with two different emission colors (composition no. 2, $\text{Ba}:\text{Si}:\text{Al} = 0.22:0.11:0.67$). (d) Microscopic image of mixed luminescent particles with three different emission colors and morphologies (composition no. 3, $\text{Ba}:\text{Si}:\text{Al} = 0.39:0.44:0.17$). (For interpretation of the references to color in this figure legend, the reader is referred to the web version of this article.)

Adapted with permission from Ref. [23]. Copyright 2014 American Chemical Society.

multilayer focusing mirrors as a monochromator operated at 50 kV and 50 mA. The absorption corrections were applied using the multiscan procedure SADABS [25]. The crystal structure was solved by direct methods implemented in SHELXL-97 [26]. Refinement of the crystal structure was carried out with anisotropic displacement parameters for all atoms by full-matrix least-squares calculation on F^2 in SHELXL-2013 [26]. The elemental analysis of cation was conducted using a scanning electron microscope (Hitachi High-technology, SU1510) equipped with an energy dispersive spectroscopy instrument (Bruker AXS, XFlash SDD) operated at 15 kV. The program VESTA was used to draw the crystal structure [27].

In the single particle fluorescence measurement, the monochromatized and focused light from a Xe lamp (Otsuka electronics, QE2100) was applied to the particle, and the luminescence from the particle was observed by a spectrometer (Otsuka electronics, MCPD7700) through a microscope (Olympus, BX51M). The calibration of the instrument was performed with a Lambertian diffuser (Labsphere, Spectralon). In the temperature dependence measurement from room temperature to 300 °C, the particle was positioned on a heater stage (Linkam Scientific Instruments, THMS600). An xyz stage was used to cancel the shift resulting from the sample movement caused by the temperature. For the quantum efficiency measurement, the particle was placed in a 1-in. integrating half sphere (Otsuka electronics, HalfMoon) and irradiated by a 405-nm laser (Thorlabs, S1FC405) through a focusing lens. The particle's absorption was obtained by subtracting the spectrum of the particle and BaSO_4 from the reflection spectrum of BaSO_4 (without the particle). The internal QE was obtained by the following equation:

$$iQE = \frac{\int \lambda \cdot P(\lambda) d\lambda}{\int \lambda \{E(\lambda) - R(\lambda)\} d\lambda}$$

where $E(\lambda)/hv$, $R(\lambda)/hv$, and $P(\lambda)/hv$ are the number of photons in the excitation, reflectance, and emission spectra of the phosphor, respectively [28].

3. Results and discussion

3.1. Ba_3N_2 - Si_3N_4 - AlN system [23]

In Ba_3N_2 - Si_3N_4 - AlN phase diagram, several phosphor hosts have been found out (Ba_7N_{10} [29], BaSi_6N_8 [30], $\text{Ba}_2\text{Si}_5\text{N}_8$ [31], $\text{Ba}_2\text{Si}_5\text{AlN}_9$ [13], etc.). However, new phosphor hosts will be left in this phase diagram and they will be discovered by the single particle diagnosis approach. Twenty samples in the Ba_3N_2 - Si_3N_4 - AlN quasi-ternary system with varying $\text{Ba}:\text{Si}:\text{Al}$ ratios (Fig. 3(a)) were prepared by firing appropriate amounts of Ba_3N_2 (Cerac, 99.7%, 20 mesh), Si_3N_4 (Ube, E-10), AlN (Tokuyama, E grade) and EuN (homemade) at 1900 °C for 2 h in 1.0 MPa N_2 atmosphere. The Eu concentration was fixed at 5 mol% with respect to Ba. The luminescence images of the UV-irradiated powders with compositions no. 1–3 are shown in Fig. 3(b)–(d). In some cases, the unreacted starting powder of Si_3N_4 or AlN was also present but had no luminescence, so that it was submerged in the background. The particles are seen to have a size of about several to several ten micrometers. Due to different growth habits the particles exhibited varying morphologies. Seven luminescent particles with different colors and morphologies were selected from the powder product. Luminescent particles with distinct colors and shapes were distinguished from the multicolored powder mixture and then individually amounted to a glass fiber for X-ray diffraction, as shown in Fig. 4.

We first identified whether the selected phosphor particle has a new crystal structure or not by using a single crystal X-ray diffractometer, followed by preliminarily calculating lattice parameters. The particle with lattice parameters not matching with those stored in database was recognized as a new crystalline phase, and it thus entered into next round of characterization. The diamond-like blue (Fig. 4(a)), plate- and diamond-like orange (Fig. 4(c) and (e)), rice grain-like red (Fig. 4(d)), and triangle blue (Fig. 4(g)) particles were identified as already known Eu^{2+} -doped Ba_7N_{10} [32], $\text{Ba}_2\text{Si}_5\text{N}_8$ [2] (diamond and plate-like), $\text{Ba}_2\text{Si}_5\text{AlN}_9$ [13] and BaSi_6N_8 [33], respectively. On the other hand, the diamond-like cyan (Fig. 4(b)) and needle-like yellow particles (Fig. 4(f)) were labeled as new phosphors with uncovered crystal

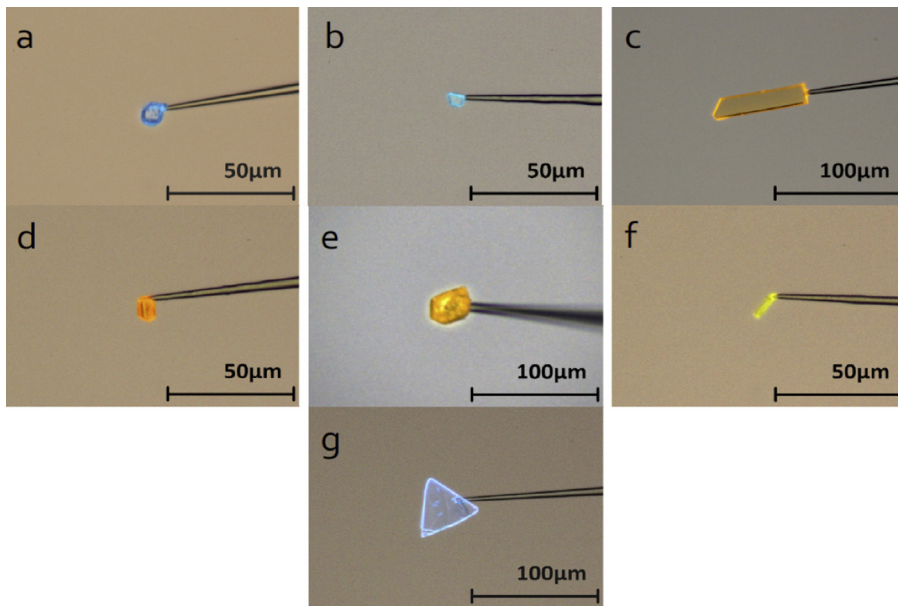


Fig. 4. Luminescent particles with different emission colors and morphologies for structural analysis. (a) Diamond-like blue particle with a size of $7 \mu\text{m} \times 7 \mu\text{m} \times 9 \mu\text{m}$ from composition no. 1. (b) Diamond-like cyan particle with a size of $4 \mu\text{m} \times 5 \mu\text{m} \times 6 \mu\text{m}$ from composition no. 2. (c) Plate-like red particle with a size of $5 \mu\text{m} \times 18 \mu\text{m} \times 80 \mu\text{m}$ from composition no. 3. (d) Rice grain-like red particle with a size of $2 \mu\text{m} \times 6 \mu\text{m} \times 8 \mu\text{m}$ from composition no. 3. (e) Diamond-like orange particle with a size of $26 \mu\text{m} \times 32 \mu\text{m} \times 35 \mu\text{m}$ from composition no. 3. (f) Needle-like yellow particle with a size of $3 \mu\text{m} \times 3 \mu\text{m} \times 10 \mu\text{m}$ from composition no. 3. (g) Triangle cyan particle with a size of $3 \mu\text{m} \times 49 \mu\text{m} \times 50 \mu\text{m}$ from composition no. 4 ($\text{Ba:Si:Al} = 0.167:0.833:0$). (For interpretation of the references to color in this figure legend, the reader is referred to the web version of this article.)

Reprinted with permission from Ref. [23]. Copyright 2014 American Chemical Society.

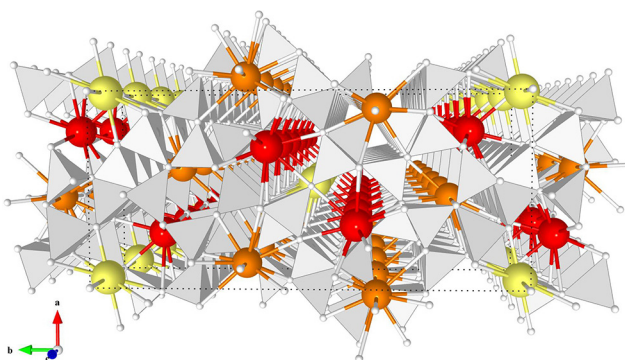


Fig. 5. Crystal structure of $\text{Ba}_5\text{Si}_{11}\text{Al}_7\text{N}_{25}:\text{Eu}^{2+}$ from the [001] direction. White tetrahedra are $(\text{Si},\text{Al})\text{N}_4$. Yellow, orange, red spheres are $\text{Ba}(\text{Eu})$, and white spheres are N. (For interpretation of the references to color in this figure legend, the reader is referred to the web version of this article.)

structures. Sixteen other compositions were identified to be either the mixture of known phases or the mixture of known phases and the unknown phase mentioned above.

The needle-like yellow particle with a size of $3 \mu\text{m} \times 3 \mu\text{m} \times 10 \mu\text{m}$ was finally refined as $\text{Ba}_5\text{Si}_{11}\text{Al}_7\text{N}_{25}:\text{Eu}^{2+}$ in the orthorhombic space group $Pnnm$ (no. 58) with $a = 9.5923(2) \text{\AA}$, $b = 21.3991(5) \text{\AA}$, $c = 5.8889(2) \text{\AA}$, and $Z = 2$ ($R_1 = 2.4\%$, $wR_2 = 5.4\%$, $S = 1.05$). The crystallographic data and structure parameters are given in the Data in Brief (Tables 1–3). The cation composition by EDS ((Ba + Eu):Si:Al = 5.0:11.0:7.0) agreed well with the structural model. Because of the similar ionic radii, Si/Al were constrained to occupy the same site, as seen in other Si/Al compounds. This new phosphor contains a highly condensed framework built-up on $(\text{Si},\text{Al})\text{N}_4$ as depicted in Fig. 5. The tetrahedra are mostly linked via common corners, but the structure also contains edge-shared tetrahedra. The framework of $\text{Ba}_5\text{Si}_{11}\text{Al}_7\text{N}_{25}$ host has three different Ba positions that are coordinated to 11 (Ba1), 10 (Ba2), and 8 (Ba3) nitrogen atoms, respectively. The Ba(Eu)-N bond lengths

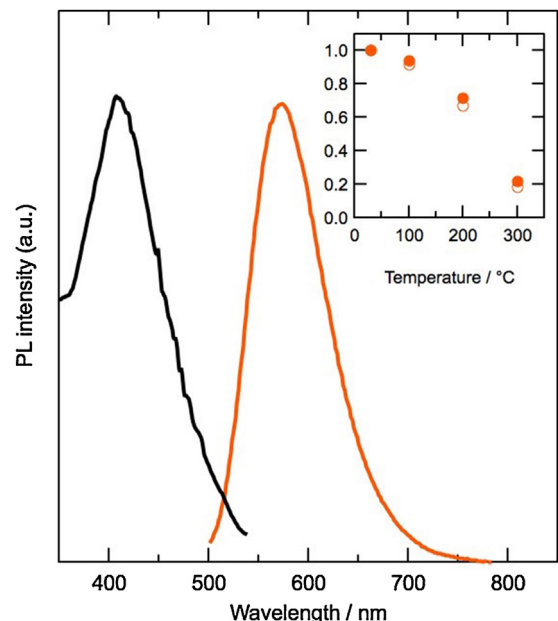


Fig. 6. Emission ($\lambda_{\text{ex}} = 400 \text{ nm}$) and excitation ($\lambda_{\text{em}} = 570 \text{ nm}$) spectra of $\text{Ba}_5\text{Si}_{11}\text{Al}_7\text{N}_{25}:\text{Eu}^{2+}$ single particle. Thermal quenching (filled: integrated intensity, open: peak intensity) is shown in the inset.

vary between $2.838(2) \text{\AA}$ and $3.030(3) \text{\AA}$ for Ba1, between $3.003(2) \text{\AA}$ and $3.354(2) \text{\AA}$ for Ba2, and between $2.719(3) \text{\AA}$ and $3.083(2) \text{\AA}$ for Ba3. The emission and excitation spectra from single particle of $\text{Ba}_5\text{Si}_{11}\text{Al}_7\text{N}_{25}:\text{Eu}^{2+}$ phosphor are shown in Fig. 6. The emission spectrum has a peak at approximately 570 nm with a broad FWHM of 98 nm . The excitation spectrum spans 350 – 550 nm . The luminescence peak intensity of the new yellow phosphor declined by 8% at 100°C and 33% at 200°C . The luminescence integrated

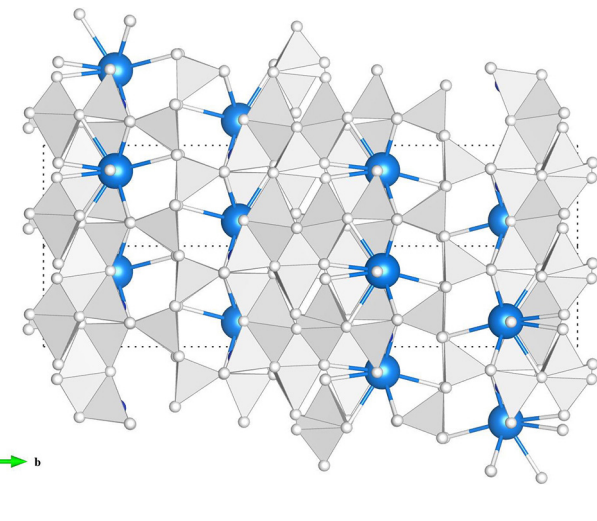


Fig. 7. Crystal structure of $\text{BaSi}_4\text{Al}_3\text{N}_9:\text{Eu}^{2+}$ from the [101] direction. White tetrahedra are $(\text{Si},\text{Al})\text{N}_4$. Blue spheres are $\text{Ba}(\text{Eu})$, and white spheres are N . (For interpretation of the references to color in this figure legend, the reader is referred to the web version of this article.)

intensity declined by 6% at 100°C and 28% at 200°C . The internal QE of the particle by 405-nm excitation was obtained to be 36%.

The diamond-like blue-emitting particle with a size of $4\text{ }\mu\text{m} \times 5\text{ }\mu\text{m} \times 6\text{ }\mu\text{m}$ was refined as $\text{BaSi}_4\text{Al}_3\text{N}_9:\text{Eu}^{2+}$ in the monoclinic space group $P2_1/c$ (no. 14) with $a = 5.8465(4)\text{\AA}$, $b = 26.7255(18)\text{\AA}$, $c = 5.8386(4)\text{\AA}$, $\beta = 118.897^\circ$, and $Z = 4$ ($R_1 = 2.0\%$, $wR_2 = 6.2\%$, $S = 1.50$). The crystallographic data and structure parameters are given in the Data in Brief (Tables 4–6). There is only one crystallographic site for Ba that is coordinated to 11 nitrogen atoms. The distances of $\text{Ba}(\text{Eu})-\text{N}$ are between $2.970(19)\text{\AA}$ and $3.497(3)\text{\AA}$, with an average length of 3.164\AA . The corner-sharing $(\text{Si},\text{Al})\text{N}_4$ tetrahedra form a layer in the a - c plane and face-sharing $(\text{Si},\text{Al})\text{N}_4$ tetrahedra in which either of the sites are occupied by Si/Al form another layer as shown in Fig. 7. Detailed local structure analysis shows the presence of staking faults in the b -axis direction [34]. Photoluminescence of a single $\text{BaSi}_4\text{Al}_3\text{N}_9:\text{Eu}^{2+}$ particle are given in Fig. 8. It showed a relatively narrow band with a peak maximum at approximately 500 nm with a FWHM of 67 nm . The excitation spectrum displayed a band with a tail extending to 450 nm . The luminescence peak intensity of the new blue phosphor declined by 6% at 100°C and 20% at 200°C . The luminescence integrated intensity declined by 2% at 100°C and 12% at 200°C . The internal QE of the particle by 405-nm excitation was obtained to be 26%.

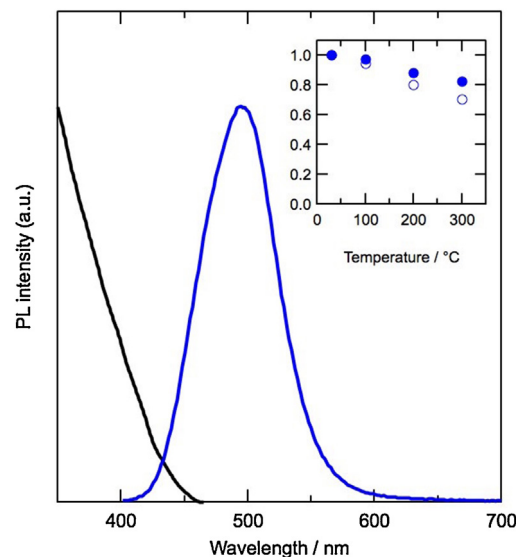


Fig. 8. Emission ($\lambda_{\text{ex}} = 350\text{ nm}$) and excitation ($\lambda_{\text{em}} = 495\text{ nm}$) spectra of $\text{BaSi}_4\text{Al}_3\text{N}_9:\text{Eu}^{2+}$ single particle. Thermal quenching (filled: integrated intensity, open: peak intensity) is shown in the inset.

In one synthesis experiment, two new phosphors were discovered by the single particle diagnosis approach.

3.2. $\text{Ba}_3\text{N}_2-\text{Li}_3\text{N}-\text{Si}_3\text{N}_4-\text{AlN}$ system [24]

We next show the result of the $\text{Ba}_3\text{N}_2-\text{Li}_3\text{N}-\text{Si}_3\text{N}_4-\text{AlN}$ quasi-quaternary system. In addition to first example, Li_3N was employed as the fourth component. As the number of components increases, the number of experiments dramatically increases in the combinatorial synthesis. In the single particle diagnosis approach, the increment of experiments number is suppressed. We have surveyed a variety of $\text{Ba}:\text{Si}:\text{Al}:\text{Li}$ cation compositions and identified a new green phosphor using a composition of $\text{Ba}:\text{Si}:\text{Al}:\text{Li} = 1.0:0.58:6.42:3.00$. The Eu (EuN) concentration was 20 mol% with respect to Ba. The mixed starting materials were fired at 1800°C for 2 h in 1.0 MPa N_2 atmosphere.

Out of the many luminescent particles as shown in Fig. 9(a), the green luminescent particle shown in Fig. 9(b) was found to be a new phosphor. It was formed as a plate shape with dimensions of $11\text{ }\mu\text{m} \times 31\text{ }\mu\text{m} \times 46\text{ }\mu\text{m}$. Although some tiny particles, which probably consist of the same new green phosphor, are present, their effect on the characterization results will be small. Other luminescent particles with different emission colors were identified

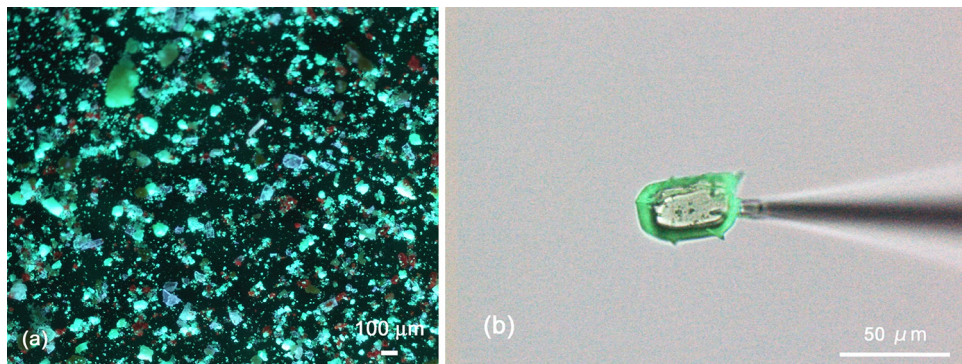


Fig. 9. Microscopic image of (a) a product generated from $\text{Ba}/\text{Si}/\text{Al}/\text{Li} = 1.0:0.58:6.42:3.00$ and (b) the selected green luminescent particle. Both images were collected under UV light. (For interpretation of the references to color in this figure legend, the reader is referred to the web version of this article.)

Adapted with permission from Ref. [24]. Copyright 2015 American Chemical Society.

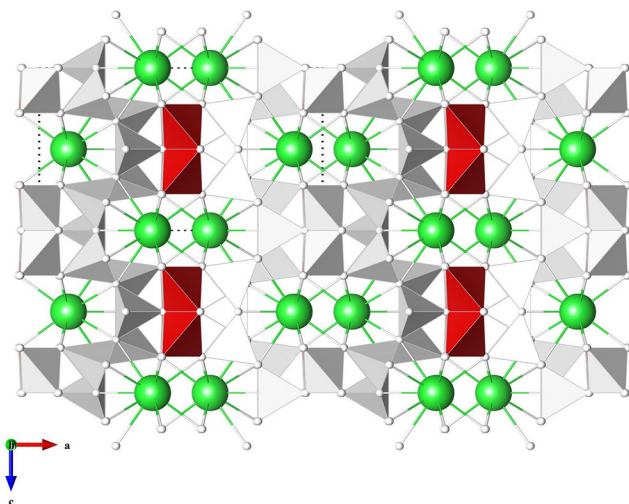


Fig. 10. Crystal structure of $\text{Ba}_2\text{LiSi}_7\text{AlN}_{12}:\text{Eu}^{2+}$ from the [010] direction. White and red tetrahedra are $(\text{Si},\text{Al})\text{N}_4$ and LiN_4 , respectively. Green spheres are $\text{Ba}(\text{Eu})$, and white spheres are N. (For interpretation of the references to color in this figure legend, the reader is referred to the web version of this article.)

as Eu^{2+} -doped $\text{BaSi}_7\text{N}_{10}$ [32] (blue emission), $\text{Ba}_2\text{Si}_5\text{N}_8$ [2] (red emission), and BaSi_6N_8 [33] (blue emission) based on single crystal XRD analysis. The single crystal XRD analysis showed that the new phosphor has an orthorhombic unit cell of $a = 14.0993(2)\text{\AA}$, $b = 4.89670(10)\text{\AA}$, $c = 8.07190(10)\text{\AA}$, and $Z = 2$ with the $Pnnm$ space group (no. 58). The crystallographic data and structure parameters are given in the Data in Brief (Tables 7–9). Considering the site multiplicity, occupancy of each site and electrical neutrality, the composition was assigned as $\text{Ba}_2\text{LiSi}_7\text{AlN}_{12}:\text{Eu}^{2+}$ ($R_1 = 1.49\%$, $wR_2 = 3.80\%$, $S = 1.047$). This value corresponds well with the cation ratio obtained by EDS analysis (($\text{Ba} + \text{Eu}$): $\text{Si}:\text{Al} = 2.0:6.9:1.1$). Because EDS cannot detect Li, LA-ICP-MASS analysis was carried out. The analysis clearly showed the presence of Li in the particle, and the Li:Si ratio was determined to be 1.4:7.0. The difference from the estimated composition is ascribed to the low accuracy of the Si content value because of N_2 contamination in the carrier gas. The bond valence sum at the Li site was calculated to be 1.0.

The crystal structure that was finally obtained is depicted in Fig. 10. Si/Al occupy the tetrahedral site (white tetrahedron), and Li occupies the independent tetrahedral site (red tetrahedron). The Li occupancy is 0.5, and either of the sites in the edge-sharing tetrahedra are occupied by Li. Vertex-sharing $(\text{Si},\text{Al})\text{N}_4$ tetrahedra form a corrugated layer along the c axis direction. Edge-sharing $(\text{Si},\text{Al})\text{N}_4$ tetrahedra and edge-sharing LiN_4 tetrahedra alternately align along the b direction and form a pillar. The corrugated layer

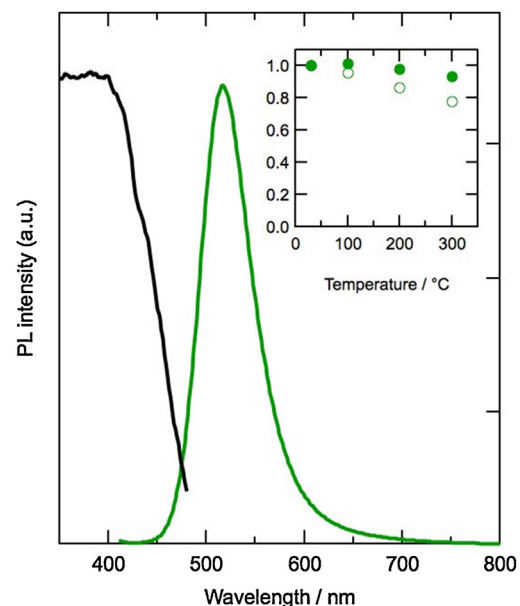


Fig. 11. Emission ($\lambda_{\text{ex}} = 400\text{ nm}$) and excitation ($\lambda_{\text{em}} = 515\text{ nm}$) spectra of $\text{Ba}_2\text{LiSi}_7\text{AlN}_{12}:\text{Eu}^{2+}$ single particle. Thermal quenching (filled: integrated intensity, open: peak intensity) is shown in the inset.

Adapted with permission from Ref. [24]. Copyright 2015 American Chemical Society.

and pillar form a large one-dimensional channel along the b direction. Ba occupies the one-dimensional channel in a zigzag manner along the b direction. There is only one crystallographic site for Ba. Ba is coordinated by eleven N atoms, and the distance between Ba and N ranges from 2.93\AA to 3.32\AA with an average distance of 3.12\AA . The BaN_{11} polyhedra are linked by face-sharing, and the distance between Ba atoms is 3.49\AA . Eu occupies the position that is 0.2\AA away from the Ba site and emits green luminescence. Eu is also coordinated by eleven N atoms, and the distance between Eu and N ranges from 2.86\AA to 3.24\AA with an average distance of 3.12\AA .

The emission and excitation spectra from single particle of $\text{Ba}_2\text{LiSi}_7\text{AlN}_{12}:\text{Eu}^{2+}$ phosphor are shown in Fig. 11. The emission spectrum has a peak at approximately 515 nm with a FWHM of 61 nm . The excitation spectrum spans 350 – 450 nm . Although the FWHM is relatively wide compared with that of very narrow green-emitting phosphor $\text{Si}_{6-z}\text{Al}_z\text{O}_z\text{N}_{8-z}:\text{Eu}^{2+}$ (55 nm), it is fairly narrow for a Eu^{2+} emitting phosphor and is suitable for backlight applications. In the powder sample, the FWHM will be reduced because the higher energy range of the emission spectrum is absorbed by other $\text{Ba}_2\text{LiSi}_7\text{AlN}_{12}:\text{Eu}^{2+}$ particles. The luminescence peak intensity of the new green phosphor declined by 4% at 100°C and 16%

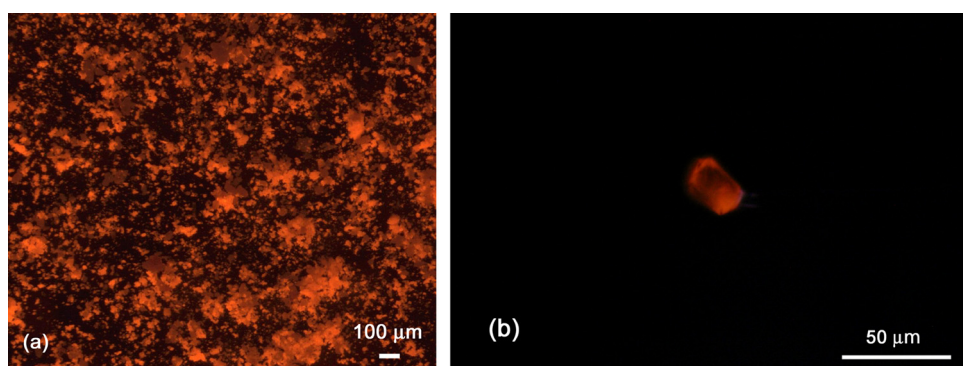


Fig. 12. Microscopic image of (a) a product generated from $\text{Ba}:\text{Si}:\text{Al} = 0.22:0.11:0.67$ and (b) the selected deep red luminescent particle. Both images were collected under UV light. (For interpretation of the references to color in this figure legend, the reader is referred to the web version of this article.)

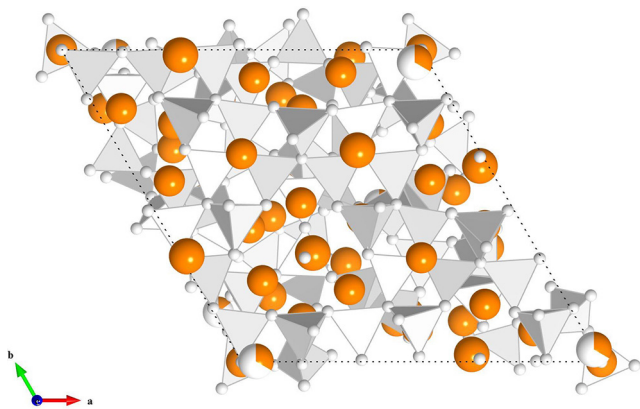


Fig. 13. Crystal structure of $(\text{La}_{26-x}\text{Sr}_x)\text{Si}_{41}(\text{O}_{1+x}\text{N}_{80-x})\text{:Eu}^{2+}$ from the [001] direction. White tetrahedra are SiN_4 . Orange spheres are $\text{La}/\text{Sr}(\text{Eu})$, and white spheres are N/O . Orange/white spheres are partially occupied site. (For interpretation of the references to color in this figure legend, the reader is referred to the web version of this article.)

at 200 °C. The luminescence integrated intensity declined by 2% at 100 °C and 5% at 200 °C. This characteristic is important for the application of high-power LED, which suffer from more predominant thermal quenching. The internal QE of the particle by 405-nm excitation was high value of 79%.

This new green phosphor will be a promising candidate for backlight applications, in which narrow-band-emitting is required, and high-power LEDs.

3.3. Sr_3N_2 – LaN – Si_3N_4 system

In the third case, we show the result of the Sr_3N_2 – LaN – Si_3N_4 quasi-ternary system. The mixed starting materials were fired at 1900 °C for 2 h in 1.0 MPa N_2 atmosphere. From a composition of $\text{Sr}:\text{La}:\text{Si} = 2.0:1.0:1.0$ (Eu_2O_3 is 1.25 mol% with respect to Sr), we found a new deep red phosphor. The luminescence images of the UV-irradiated powders showed two kinds of luminescence (orange and deep red) as shown in Fig. 12(a). The orange luminescent particle was identified as Eu^{2+} -doped $\text{Sr}_2\text{Si}_5\text{N}_8$ [2] and the deep red luminescent particle was found to be a new phosphor. The new phosphor was formed as a rectangular shape with dimensions of $17 \mu\text{m} \times 21 \mu\text{m} \times 28 \mu\text{m}$ as shown in Fig. 12(b). Because the luminescence intensity is weak, the image was taken without microscope illumination. The single crystal XRD analysis showed that the new phosphor has a hexagonal unit cell of $a = 17.3506(5) \text{\AA}$, $c = 22.4052(6) \text{\AA}$, and $Z = 3$ with the $P-6$ space group (no. 174). The crystallographic data and structure parameters are given in the Data in Brief (Tables 10–11). There are 21 independent Sr/La sites and 24 independent Si sites. Sr/La ratio were refined in each site and the chemical composition was obtained as $(\text{La}_{26-x}\text{Sr}_x)\text{Si}_{41}(\text{O}_{1+x}\text{N}_{80-x})\text{:Eu}^{2+}$ ($x = 12.81$) from the refined value ($R_1 = 7.4\%$, $wR_2 = 17.0\%$, $S = 1.054$). The oxygen contamination will be due to Eu_2O_3 and oxygen impurity in starting material of Si_3N_4 . The cation ratio almost corresponded with the EDS analysis ($\text{La}:\text{Sr}:\text{Si} = 9.6:11.6:41.0$). The crystal structure that was finally obtained is depicted in Fig. 13. The corner-sharing SiN_4 tetrahedra form complex three dimensional network and La, Sr are coordinated by 9–11 anions.

The emission and excitation spectra from one particle of $(\text{La}_{26-x}\text{Sr}_x)\text{Si}_{41}(\text{O}_{1+x}\text{N}_{80-x})\text{:Eu}^{2+}$ phosphor are shown in Fig. 14. The emission spectrum has a peak at approximately 656 nm with a FWHM of 120 nm and the excitation spectrum spans 380–550 nm. The QE by 405-nm excitation was less than 1%, coinciding with the difficulty of the image acquisition. The excitation band of Eu may be close or overlap to the conduction band of matrix.

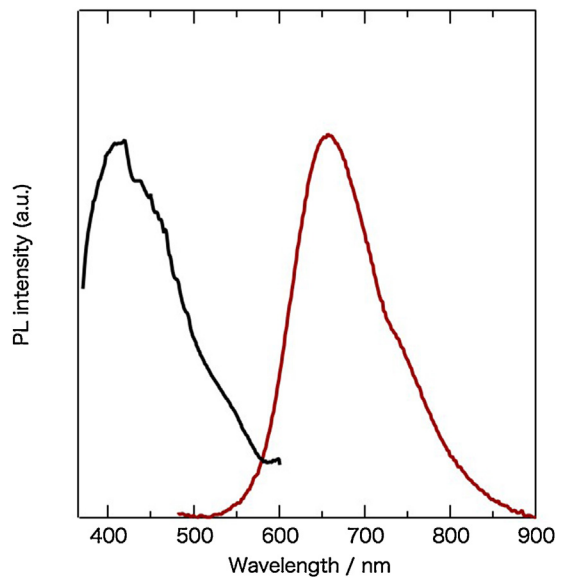


Fig. 14. Emission ($\lambda_{\text{ex}} = 400 \text{ nm}$) and excitation ($\lambda_{\text{em}} = 680 \text{ nm}$) spectra of $(\text{La}_{26-x}\text{Ba}_x)\text{Si}_{41-y}\text{Al}_y(\text{O}_{1+x+y}\text{N}_{80-x-y})\text{:Eu}^{2+}$ single particle.

4. Conclusions

The single particle diagnosis approach for new phosphor discovery was explained with some examples. In this approach, one particle in the powder product synthesized without special process is treated as a candidate for new phosphor. There is no need to synthesize a phase-pure powder or grow the large crystal of new phosphor as necessary in the conventional approach. This approach can considerably speed up the discovery of new phosphor and find the new phosphor overlooked in the conventional method. As in the example 2, this approach is easily applicable to the complex multi-nary compound because the new material particle is included in the wide composition range in the phase diagram. The problem is that the process for powder synthesis (scale up) is not clear. However, the existence of new phosphor is assured and the detailed experiments will reach the new phosphor powder.

Here we show the results of Si, Al containing nitride and oxynitride phosphors for white LEDs application. Unambiguously, our approach can also be applicable to other luminescent material systems such as oxides, fluorides, sulfides, etc. Prospectively, it seems feasible to apply our concept to other solid state materials such as catalytic, magnetic, dielectric, thermoelectric and battery materials, given that corresponding microscale characterization techniques are available.

Appendix A. Supplementary data

Supplementary data associated with this article can be found, in the online version, at [doi:10.1016/j.md.2015.11.001](https://doi.org/10.1016/j.md.2015.11.001).

References

- [1] K. Uheda, N. Hirosaki, Y. Yamamoto, A. Naoto, T. Nakajima, H. Yamamoto, *Electrochim. Solid State Lett.* 9 (2006) H22–H25.
- [2] Y.Q. Li, J.E.J. Steen, J.W.H. Krevel, G. Botty, A.C.A. Delsing, F.J. Disalvo, G. With, H.T.J. Hintzen, *J. Alloys Compd.* 417 (2006) 273–279.
- [3] R.-J. Xie, N. Hirosaki, K. Sakuma, Y. Yamamoto, M. Mitomo, *Appl. Phys. Lett.* 84 (2004) 5404–5406.
- [4] N. Hirosaki, R.-J. Xie, K. Kimoto, T. Sekiguchi, Y. Yamamoto, T. Suehiro, M. Mitomo, *Appl. Phys. Lett.* 86 (2005) 211905.
- [5] P. Pust, V. Weiler, C. Hecht, A. Tucks, A.S. Wochnik, A.K. Henß, D. Wiechert, C. Scheu, P.J. Schmidt, W. Schnick, *Nat. Mater.* 13 (2014) 891–896.
- [6] S. Schmiechen, H. Schneider, P. Wagatha, C. Hecht, P.J. Schmidt, W. Schnick, *Chem. Mater.* 24 (2014) 2712–2719.

- [7] P. Pust, A.S. Wochnik, E. Baumann, P.J. Schmidt, D. Wiecher, C. Scheu, W. Schnick, *Chem. Mater.* 24 (2014) 3544–3548.
- [8] R. Mueller-Mach, G. Mueller, M.R. Krames, H.A. Höppe, F. Stadler, W. Schnick, T. Juestel, P. Schmidt, *Phys. Stat. Sol. (a)* 202 (2005) 1727–1732.
- [9] Y. Fukuda, K. Ishida, I. Mitsuishi, S. Nunoue, *Appl. Phys. Express* 2 (2009) 012401.
- [10] O. Oeckler, J.A. Kechele, H. Koss, P.J. Schmidt, W. Schnick, *Chem. Eur. J.* 15 (2009) 5311–5319.
- [11] K. Shioi, Y. Michiue, N. Hirosaki, R.-J. Xie, T. Takeda, Y. Matsushita, M. Tanaka, Y.Q. Li, *J. Alloys Compd.* 509 (2011) 332–337.
- [12] F. Hintze, F. Hummel, P.J. Schmidt, D. Wiechert, W.W. Schnick, *Chem. Mater.* 24 (2012) 402–407.
- [13] J.A. Kechele, C. Hecht, O. Oeckler, J.S. Gunne, P.J. Schmidt, W. Schnick, *Chem. Mater.* 21 (2009) 1288–1295.
- [14] H.A. Hoppe, H. Lutz, P. Morys, W. Schnick, A.J. Seilmeyer, *Phys. Chem. Solids* 61 (2000) s2001–s2006.
- [15] M. Mikami, S. Shimooka, K. Uheda, J. Imura, N. Kijima, *Key Eng. Mater.* 403 (2009) 11–14.
- [16] E. Danielson, J.H. Golden, E.W. McFarland, C.M. Reaves, W.H. Weinberg, X.D. Wu, *Nature* 389 (1997) 944–948.
- [17] X.D. Sun, K.A. Wang, Y. Yoo, W.G. Wallace-Freedman, C. Gao, X.-D. Xiang, P.G. Schultz, *Adv. Mater.* 9 (1997) 1046–1049.
- [18] E. Danielson, M. Devenney, D.M. Giaquinta, J.H. Golden, R.C. Haushalter, E.W. McFarland, D.M. Poojary, C.M. Reaves, W.H. Weinberg, X.D. Wu, *Science* 279 (1998) 837–839.
- [19] J. Wang, Y. Yoo, C. Gao, I. Takeuchi, X.D. Sun, H. Chang, X.-D. Xiang, *Science* 279 (1998) 1712–1714.
- [20] W.B. Park, S.P. Singh, C. Yoon, K.S. Sohn, *J. Mater. Chem.* 22 (2012) 14068–14075.
- [21] K.H. Son, S.P. Singh, K.S. Sohn, *J. Mater. Chem.* 22 (2012) 8505–8511.
- [22] W.B. Park, N. Shin, K.P. Hong, M. Pro, K.S. Sohn, *Adv. Funct. Mater.* 22 (2012) 2258–2266.
- [23] N. Hirosaki, T. Takeda, S. Funahashi, R.-J. Xie, *Chem. Mater.* 26 (2014) 4280–4288.
- [24] T. Takeda, N. Hirosaki, S. Funahashi, R.-J. Xie, *Chem. Mater.* 27 (2015) 5892–5898.
- [25] G.M. Sheldrick, GSADABS, v. 2: Multi-Scan Absorption Correction, Bruker-AXS, WA, 2012.
- [26] G.M. Sheldrick, *Acta Cryst. A* 64 (2008) 112–122.
- [27] K. Momma, F. Izumi, *J. Appl. Crystallogr.* 44 (2011) 1272–1276.
- [28] K. Ohkubo, Y. Nakagawa, *J. Light Vis. Environ.* 37 (2013) 16–27.
- [29] H. Huppertz, W. Schnick, *Chem. Eur. J.* 3 (1997) 252–259.
- [30] F. Stadler, O. Oeckler, J. Senker, H.A. Höppe, P. Kroll, W. Schnick, *Angew. Chem. Int. Ed.* 44 (2005) 567–570.
- [31] T. Schlieper, W. Milius, W. Schnick, Z. Anorg. Allg. Chem. 621 (1995) 1380–1384.
- [32] Y.Q. Li, A.C.A. Delsing, R. Metslaar, G. With, H.T.J. Hintzen, *J. Alloys Compd.* 487 (2009) 28–33.
- [33] K. Shioi, N. Hirosaki, R.-J. Xie, T. Takeda, Y.Q. Li, *J. Mater. Sci.* 43 (2008) 5659–5661.
- [34] H. Yamane, F. Yoshimura, *J. Solid State Chem.* 228 (2015) 258–265.